PROFESSOR WENZHONG LU (Orcid ID : 0000-0003-1164-0233)

DR WEN LEI (Orcid ID : 0000-0003-1164-0233)

Article type : Article

Crystal structure, phase compositions, and microwave dielectric properties of malayaite-type $Ca_{1-x}Sr_xSnSiO_5$ ceramics

Kang Du[a], Jun Fan[a], Zheng-Yu Zou[a], Xiao-Qiang Song[a], Wen-Zhong Lu[a,b], Wen Lei[a,b]*

[a] School of Optical and Electronic Information, Key Lab of Functional Materials for Electronic Information (B) of MOE, Huazhong University of Science and Technology, Wuhan 430074, P. R. China

[b] Wuhan National Laboratory for Optoelectronics, Huazhong University of Science and Technology, Wuhan 430074, P. R. China

Abstract

Low-permittivity $Ca_{1-x}Sr_xSnSiO_5$ ($0 \le x \le 0.45$) microwave dielectric ceramics were prepared via traditional state-reaction at 1400 °C–1450 °C for 5 h. Moreover, the microwave dielectric properties of SnO_2 ceramic were obtained for the first time. SnO_2 ceramic was difficult to densify, and SnO_2 ceramic (ρ_{rel} = 65.1%) that was sintered at 1525 °C exhibited the optimal microwave dielectric properties of ε_r = 5.27, $Q \times f$ = 89,300 GHz (at 14.5 GHz), and τ_f = −26.7 ppm/°C. For $Ca_{1-x}Sr_xSnSiO_5$ ($0 \le x \le 0.15$) ceramics, Sr^{2+} could be dissolved in the Ca^{2+} site of $Ca_{1-x}Sr_xSnSiO_5$

* Corresponding author. Tel.: +86 27 8755 6493; fax: +86 27 8754 3134.
E-mail address: wenlei@mail.hust.edu.cn (W. Lei)

This article has been accepted for publication and undergone full peer review but has not been through the copyediting, typesetting, pagination and proofreading process, which may lead to differences between this version and the Version of Record. Please cite this article as doi: 10.1111/jace.17360

to form a single phase, and the partial substitution of Ca^{2+} by Sr^{2+} could improve the microwave dielectric properties of $CaSnSiO_5$ ceramic. Secondary phases (SnO_2 and $SrSiO_3$) appeared at $0.2 \leq x \leq 0.45$ and could adjust the abnormally positive τ_f value of $CaSnSiO_5$ ceramic. The highest $Q\times f$ value (60,100 GHz at 10.4 GHz) and optimal microwave dielectric properties (ε_r = 9.42, $Q\times f$ = 47,500 GHz at 12.4 GHz, and τ_f = −1.2 ppm/°C) of $Ca_{1-x}Sr_xSnSiO_5$ ceramics were obtained at x = 0.05 and 0.45, respectively.

Keywords: $CaSnSiO_5$ ceramic; crystal structure; phase composition; microwave dielectric properties

1. Introduction

$CaSnSiO_5$, commonly known as malayaite, is a rare mineral that has elicited considerable research interest because of its excellent photoluminescence properties.[1] The crystal structure of $CaSnSiO_5$ was first established by Higgins and Ribbe.[2] Its corner-sharing SnO_6 octahedral chains are parallel to the *a* axis and linked to CaO_7 polyhedrons via SiO_4 tetrahedrons.[3,4] The properties of $CaSnSiO_5$ are mainly affected by its SnO_6 octahedral chains. The crystal structure of $CaSnSiO_5$ is similar to that of $CaTiSiO_5$ (titanite), which has a $P2_1/a$ space group and antiferroelectirc properties at room temperature due to the Ti atom of the TiO_6 octahedron located in the off-center position.[5] However, the Sn atom (r_{Sn} = 0.83 Å) is larger than the Ti atom (r_{Ti} = 0.745 Å)[6] and more likely to occupy the central position of the octahedron.[3] Meanwhile, $CaSnSiO_5$ has a monoclinic structure with an $A2/a$ space group and is not an antiferroelectirc ceramic at room temperature.[2]

The applications of low-permittivity $CaSnSiO_5$ microwave dielectric ceramic are attracting increased attention because of its large number of Si–O bonds and abnormally positive τ_f value.[7,8] Silicates possess numerous Si–O bonds (approximately 55% covalent bonds) in their SiO_4 tetrahedrons and exhibit low permittivity (ε_r < 15),[9] which can decrease signal transmission time. Ternary silicate ceramics such as $CaO\text{-}SnO_2\text{-}SiO_2$,[10,11] $CaO\text{-}ZrO_2\text{-}SiO_2$,[12,13] $CaO\text{-}HfO_2\text{-}SiO_2$[13] also have a high-quality factor ($Q\times f$). High $Q\times f$ values can improve frequency selectivity[14] and high bond relative covalency corresponds to a high $Q\times f$ value.[10,13] Moreover, low-permittivity

microwave dielectric ceramics with a positive temperature coefficient of resonant frequency (τ_f) based on the ε_r–τ_f relationship are rare.[15] In the CaO–SnO_2–SiO_2 system, only $CaSnSiO_5$ and $Ca_3SnSi_2O_9$ ternary oxides exist. $CaSnSiO_5$ and $Ca_3SnSi_2O_9$ ceramics exhibit high $Q\times f$ values and low permittivity,[7,11] and only $CaSnSiO_5$ ceramic possess an abnormally large positive τ_f values. In our previous work, the microwave dielectric properties and phase compositions of $CaSnSiO_5$ ceramic were carefully investigated. However, due to the high relative covalency (approximately 53%) of the Sn–O bond of the SnO_6 octahedral chains in $CaSnSiO_5$, improving the relative covalency of the Sn–O bond and the $Q\times f$ values of $CaSnSiO_5$ ceramic via Sn^{4+} substitution is difficult. Thus, how to improve the microwave dielectric properties of $CaSnSiO_5$ ceramic is worthy of further research.

In the present work, $Ca_{1-x}Sr_xSnSiO_5$ ($0 \leq x \leq 0.45$) microwave dielectric ceramics were investigated. The bond length of Sn–O was compressed and the relative covalency of Sn-O increased through Ca^{2+} substitution by the larger Sr^{2+}. The partial substitution of Ca^{2+} by Sr^{2+} improved the microwave dielectric properties of $CaSnSiO_5$. Phase compositions and crystal structure were analyzed through Rietveld refinement. The microwave dielectric properties of $Ca_{1-x}Sr_xSnSiO_5$ ($0 \leq x \leq 0.15$) ceramics were primarily affected by ionic polarizability, bond relative covalency content, microstructure, and SnO_6 octahedral distortion in single-phase area. In multi-phase area, the secondary phase was a key factor that affected the microwave dielectric properties of $Ca_{1-x}Sr_xSnSiO_5$ ($0.2 \leq x \leq 0.45$) ceramics.

2. Experimental

$Ca_{1-x}Sr_xSnSiO_5$ ($0 \leq x \leq 0.45$) and SnO_2 ceramics were prepared through solid-state reaction by using $CaCO_3$ (99.5%), SnO_2 (99.9%), and SiO_2 (99.5%) powders as raw materials. The raw powders were weighed in accordance with stoichiometry and mixed by milling for 5 h with zirconia balls in a polyethylene jar containing deionized water. After drying at 80 °C, final powders were calcined at 1150 °C for 10 h at a heating rate of 5 °C/min. Then, the calcined powders were remilled for 5 h and dried again. Fine powders were pressed with 8 wt% PVA solution into samples with a diameter of 12 mm and thickness of 6 mm under a pressure of 150

MPa. Finally, the samples were sintered in air at 1400 °C–1525 °C for 5 h at a heating rate of 5 °C/min and then cooled down to 1000 °C at a rate of 1 °C/min.

The bulk density of the ceramics was measured by using the Archimedes method. Relative density (ρ_{rel}) was obtained with Formula (1).[16]

$$\rho_{rel} = \frac{\rho_{obs}}{\rho_{the}} \tag{1}$$

where ρ_{obs} and ρ_{the} are the bulk and theoretical densities, respectively. ρ_{the} can be obtained on the basis of Rietveld refinement results.

The ρ_{rel} of mul-phase ceramics can be calculated with Formula (2).

$$\rho_{the} = \frac{W_1 + W_2}{W_1 / \rho_1 + W_2 / \rho_2} \tag{2}$$

where W_1 and W_2 are the weight percentages and ρ_1 and ρ_2 are the theoretical densities of phases 1 and 2, respectively.

Phase compositions were confirmed through X-ray diffraction (XRD–7000, Shimadzu, Kyoto, Japan) with CuKα radiation. Phase analysis and evolution of crystal structure were performed by Rietveld refinement using FullProf software.[17] The microstructures of the thermally etched ceramics were observed via scanning electron microscopy (SEM; Sirion 200, the Netherlands). Thermal etching was conducted at 100 °C below densification temperatures for 30 min.

Microwave dielectric properties were evaluated by using a network analyzer (Agilent E8362B, Agilent Technologies, USA). ε_r and unloaded $Q \times f$ values were measured through the Hakki and Coleman method.[18] τ_f was calculated by formula (3).

$$\tau_f = \frac{1}{f(T_0)} \frac{[f(T_1) - f(T_0)]}{T_1 - T_0} \tag{3}$$

where $f(T_1)$ and $f(T_0)$ are the resonant frequencies at T_1 (80 °C) and T_0 (20 °C), respectively.

3. Results and discussion

Fig. 1 shows the XRD patterns of $Ca_{1-x}Sr_xSnSiO_5$ ($0 \leq x \leq 0.45$) ceramics sintered at

optimized temperatures. Single-phase ceramics were obtained at $0 \leq x \leq 0.15$ and exhibited the $CaSnSiO_5$ phase (JCPDS No. 86-0928) with a monoclinic structure and $A2/a$ space groups. At $0 \leq x \leq 0.15$, the XRD patterns of $Ca_{1-x}Sr_xSnSiO_5$ ceramics shifted to low angles with the increase in x due to Ca^{2+} (r_{Ca}^{2+} = 1.06 Å) substitution by Sr^{2+} (r_{Sr}^{2+} = 1.21 Å) with the larger ionic radius. With the increase in x, the SnO_2 (JCPDS No. 21-1250) and $SrSiO_3$ (JCPDS No. 36-0018) secondary phases appeared at $0.3 \leq x \leq 0.45$, and the intensity of the SnO_2 and $SrSiO_3$ diffraction peaks increased gradually, indicating the increased content of the secondary phase in $Ca_{1-x}Sr_xSnSiO_5$ ceramics. As shown in Fig. 1, SnO_2 single-phase ceramic was also prepared. However, it was difficult to determine phase compositions at x = 0.2 by XRD patterns. The maximum solubility of $Ca_{1-x}Sr_xSnSiO_5$ appeared to be located at 0.2.

To further examine the maximum solubility, content of the secondary phase, and lattice structure of $Ca_{1-x}Sr_xSnSiO_5$ ceramics, Rietveld refinement was conducted. The refinement diffraction figure of $CaSnSiO_5$ (x = 0) ceramic has been provided in our previous article,[8] and Fig. 2 shows the refined diffraction figure of $Ca_{1-x}Sr_xSnSiO_5$ ceramics (x = 0.05, 0.1, and 0.15). The calculated refinement results agreed well with the measured diffraction profiles, and no secondary phase was observed in Fig. 2. The refinement results of $Ca_{1-x}Sr_xSnSiO_5$ ($0 \leq x \leq 0.45$) and SnO_2 ceramics are listed in Table 1. The goodness-of-fit indicator χ^2 values confirmed the reliability of the Rietveld refinement results. At $0 \leq x \leq 0.15$, lattice parameters (a, b, c, and β) and unit cell volumes gradually increased with the increase in x as a result of the substitution of Sr^{2+} for Ca^{2+}. The SnO_2 secondary phase (4.8 *wt*%) was observed at x = 0.2 from the results of Rietveld refinement. Thus, the maximum solubility of $Ca_{1-x}Sr_xSnSiO_5$ was located between 0.15 and 0.2. With the further increase in x, the weight percentages of the SnO_2 and $SrSiO_3$ secondary phases increased and the SnO_2 phase became a main phase at x = 0.45. At $0.2 \leq x \leq 0.45$, lattice parameters (a, b, c, and β) and unit cell volumes did not a linearly change with the increase in x due to the appearance of the secondary phase.

Table 2 shows the bond length (d) of $Ca_{1-x}Sr_xSnSiO_5$ ($0 \leq x \leq 0.15$) ceramics from Rietveld refinement results. The average bond length of Ca/Sr–O increased to the maximum values at x = 0.15 because Sr^{2+} with the larger ionic radius occupied the Ca^{2+} sites, and the average bond length

of Si–O showed a downward trend as a function of *x*. However, the average bond length of Sn–O decreased to the minimum value at $x = 0.05$ and then increased slightly. Ca/Sr–O was the longest and weakest chemical bond in $Ca_{1-x}Sr_xSnSiO_5$ ceramics. Ca^{2+} had a coordination number of 7, and was connected with one O_1 atom, two O_2 atoms, and four O_3 atoms. Ca–O_1 was the shortest chemical bond amongst all Ca–O bonds, indicating that Ca–O_1 was stronger than Ca–O_2 and Ca–O_3. The coordination number for Sn^{4+} was 6, and the average bond length of Sn–O was between that of Ca–O and Si–O. The average bond length of Sn–O_1 was affected by Ca–O_1 and exhibited a variation trend that opposed that shown by Ca–O_1 with the increase in *x*. Si^{4+}had a coordination number of 4 and was connected with two O_2 and two O_3 atoms. Si–O was the shortest and strongest chemical bond in $Ca_{1-x}Sr_xSnSiO_5$ ceramics because of the high electronegativity of Si.[19]

Fig. 3 shows the SEM images of $Ca_{1-x}Sr_xSnSiO_5$ ($0 \le x \le 0.45$) and SnO_2 ceramics, as well as the energy-dispersive spectroscopy (EDS) images of $Ca_{1-x}Sr_xSnSiO_5$ ($0 \le x \le 0.15$). Dense microstructures were observed in $Ca_{1-x}Sr_xSnSiO_5$ ($0 \le x \le 0.3$) ceramics. A porous microstructure existed in $Ca_{1-x}Sr_xSnSiO_5$ ($x = 0.45$) and SnO_2 ceramics. At $x = 0$, the average grain size of $CaSnSiO_5$ single-phase ceramic was approximately 3 μm and not uniform. With the substitution of Ca^{2+} by Sr^{2+}, the average grain size of $Ca_{1-x}Sr_xSnSiO_5$ ceramics increased (approximately 5 μm) and homogenous microstructure appeared at $x = 0.05$. Consistent with the results of Rietveld refinement, no obvious secondary phases were detected at $0 \le x \le 0.15$. With the further increase in *x*, the average grain size of $Ca_{1-x}Sr_xSnSiO_5$ ($0.15 < x \le 0.45$) ceramics decreased slightly, and an obvious SnO_2 secondary phase was observed at $x = 0.45$. The maximum average grain size of SnO_2 was approximately 10 μm (Fig. 3 (h)). EDS results confirmed that Ca^{2+} was occupied by Sr^{2+} to form a solid solution in $Ca_{1-x}Sr_xSnSiO_5$ ($0.05 \le x \le 0.15$) ceramics. The ratio of Ca:Sr:Sn:Si:O was approximately consistent with the composition of $Ca_{1-x}Sr_xSnSiO_5$ ($0 \le x \le 0.15$) ceramics and the presence of the SnO_2 secondary phase in $Ca_{0.55}Sr_{0.45}SnSiO_5$ ceramic was confirmed by EDS results (Spot E).

Table 3 shows the optimized sintered temperature, relative densities (ρ_{rel}), total ionic polarizability (α_D^T), and microwave dielectric properties of $Ca_{1-x}Sr_xSnSiO_5$ ($0 \le x \le 0.45$), SnO_2, and $SrSiO_3$ ceramics. The optimized sintered temperature of $Ca_{1-x}Sr_xSnSiO_5$ ceramics decreased

after the substitution of Sr^{2+} for Ca^{2+} and then increased slightly due to the large number of SnO_2 and $SrSiO_3$ secondary phases that had appeared. The optimized sintered temperature of SnO_2 and $SrSiO_3$ ceramics were above 1500 °C. With the increase in x, the ρ_{rel} of $Ca_{1-x}Sr_xSnSiO_5$ ($0 \le x \le 0.45$) ceramics initially increased and then decreased. The ρ_{rel} of single-phase $Ca_{1-x}Sr_xSnSiO_5$ ($0 \le x \le 0.15$) ceramics increased gradually with x, and the ρ_{rel} of multi-phase ceramics presented a reducing tendency at $0.2 \le x \le 0.45$. The slight substitution of Sr^{2+} for Ca^{2+} could improve the ρ_{rel} of $Ca_{1-x}Sr_xSnSiO_5$ ceramics, and the appearance of the SnO_2 secondary phase could increase porosity. $\varepsilon_{r\text{-}exp}$ values tended to increase initially and then decreased, whereas τ_f values decreased gradually with the increase in x. Moreover, $Q \times f$ values did not linearly change.

At the single-phase area, the effects of ρ_{rel} on microwave dielectric properties could be eliminated because the ρ_{rel} of $Ca_{1-x}Sr_xSnSiO_5$ ($0 \le x \le 0.15$) ceramics exceeded 95%. The $\varepsilon_{r\text{-}exp}$ of $Ca_{1-x}Sr_xSnSiO_5$ ($0 \le x \le 0.15$) ceramics depended mainly on total ionic polarizability and calculated relative permittivity ($\varepsilon_{r\text{-}cal}$). $\varepsilon_{r\text{-}cal}$ was calculated by using the Clausius-Mossotti formulas (4) and (5).[21,22]

$$\varepsilon_{r-cal} = \frac{1 + 2b\alpha_D^T / V_m}{1 - b\alpha_D^T / V_m} \tag{4}$$

$$\alpha_D^T = (1-x)\alpha\left(Ca^{2+}\right) + x\alpha\left(Sr^{2+}\right) + \alpha\left(Sn^{4+}\right) + \alpha\left(Si^{4+}\right) + 5\alpha\left(O^{2-}\right) \tag{5}$$

where $\alpha\left(Ca^{2+}\right) = 3.16$ Å^3, $\alpha\left(Sr^{2+}\right) = 4.24$ Å^3, $\alpha\left(Sn^{4+}\right) = 2.83$ Å^3, $\alpha\left(Si^{4+}\right) = 0.87$ Å^3, and $\alpha\left(O^{2-}\right) = 2.01$ Å^3 are the ionic polarizabilities; $b = 4\pi/3$; and V_m is the molar volume from the results of Rietveld refinement.

To eliminate the effects of porosity on $\varepsilon_{r\text{-}exp}$, the corrected relative permittivity ($\varepsilon_{r\text{-}corr}$) was calculated through formulas (6) and (7).[23]

$$\varepsilon_{r-corr} = \varepsilon_{r-\exp}(1 + 1.5P) \tag{6}$$

$$P = 1 - \rho_{rel} \tag{7}$$

where P is porosity.

The Lichtenecker empirical rule[24] was used to calculate the $\varepsilon_{r\text{-}cal}$ values of multi-phase

$Ca_{1-x}Sr_xSnSiO_5$ ($0.2 \le x \le 0.45$) ceramics.

$$\ln \varepsilon_{r-cal} = V_1 \ln \varepsilon_{r-1} + V_2 \ln \varepsilon_{r-2} + V_3 \ln \varepsilon_{r-3} \quad (8)$$

where V_i and ε_{r-i} are the volume fraction and calculated relative permittivity of the *i*th phase.

As shown in Table 3 and Fig. 4, the variation trend of ε_{r-exp} was the same as that of total ionic polarizability and ε_{r-cal} in the single-phase area. The ε_{r-exp} values of multi-phase $Ca_{1-x}Sr_xSnSiO_5$ ($0.2 \le x \le 0.45$) ceramics were affected mostly by the secondary phase. The appearance of the SnO_2 secondary phase could increase porosity and decrease ε_{r-exp}. In the multi-phase area, the ε_{r-exp} of $Ca_{1-x}Sr_xSnSiO_5$ ($0.2 \le x \le 0.45$) ceramics was dominated by the relative density and ε_{r-exp} of second-phase ceramics rather than total ionic polarizability.

To investigate the effect of Sr^{2+} substitution for Ca^{2+} on the crystal structure, The SnO_6 octahedral distortion and the relative covalency of cation-oxygen bonds were calculated on the basis of the bond-length data from Rietveld refinement (Table 2). The bond valence of cation was calculated by using Formulas (9) and (10).[25,26]

$$V_i = \sum_j v_{ij} \quad (9)$$

$$v_{ij} = \exp\left(\frac{R_{ij} - d_{ij}}{n}\right) \quad (10)$$

where d_{ij} is the bond length between *i* and *j* atoms (Table 2), R_{ij} is the bond-valence parameters ($R_{Ca\text{-}O}$ = 1.967 Å, $R_{Sr\text{-}O}$ = 2.118 Å, $R_{Sn\text{-}O}$ = 1.905 Å, and $R_{Si\text{-}O}$ = 1.624 Å),[25] and the constant of *n* is 0.37.

The ratio of the bond-valence sum and its coordination number was used to calculate bond strength (*S*), and relative covalency was calculated with Formulas (11) and (12).[27]

$$f_c = gS^m \quad (11)$$

$$\text{Relative Covalency (\%)} = \frac{f_c}{S} \times 100 \quad (12)$$

where *g* and *m* are the empirical parameters[26] determined by the number of electrons in the cation core.

The atomic interactions of $CaSnSiO_5$ ceramic was modified because of Sr^{2+} substitution for Ca^{2+}. The variation trend of the bond length of Ca/Sr–O generally opposed that of the bond length

of Sn–O, except for a few unmatched numbers, which resulted in a change in the SnO_6 octahedron. SnO_6 octahedral distortion (δ) was calculated by using Formula (13).[28]

$$\delta = \frac{1}{6}\sum(\frac{d_i - \bar{R}}{\bar{R}})^2 \quad (13)$$

where $\bar{R}$ and d_i are the average and individual bond lengths of the Sn–O bond, respectively.

Table 4 shows the distortion of the SnO_6 octahedron, the bond valence of cations, and relative covalency of the cation-oxygen bonds of $Ca_{1-x}Sr_xSnSiO_5$ ($0 \le x \le 0.15$) ceramics. High bond valence corresponded to large relative covalency. The largest relative covalency (above 55%) was obtained for Si–O bonds in the SiO_4 tetrahedron and corresponded to the shortest bond length. Fig. 5 shows the variation trend of the relative covalency of Sn–O bonds and $Q\times f$ values as a function of x. Generally, $Q\times f$ values are influenced not only by intrinsic factors such as lattice vibrational modes, but also by extrinsic factors such as pores, secondary phases, lattice defects, and inner stress.[29] In $Ca_{1-x}Sr_xSnSiO_5$ ($0 \le x \le 0.15$) single-phase ceramics, the large relative covalency of bonds and homogenous microstructure (Fig. 2) were responsible for high $Q\times f$ values,[13] and the highest $Q\times f$ values was obtained for $Ca_{1-x}Sr_xSnSiO_5$ ($x = 0.05$) ceramic. The variation trend of the $Q\times f$ values of $Ca_{1-x}Sr_xSnSiO_5$ ($0 \le x \le 0.15$) ceramics was the same as that of the relative covalency of Sn–O. In the multi-phase area, $Q\times f$ values initially decreased and then increased, which was primarily affected by the secondary phase. The appearance of the secondary phase could deteriorate $Q\times f$ values at ($0.2 \le x \le 0.4$), and the increase in the $Q\times f$ values of $Ca_{1-x}Sr_xSnSiO_5$ ($x = 0.45$) ceramic could be attributed to random error.

The τ_f values of $Ca_{1-x}Sr_xSnSiO_5$ ($0 \le x \le 0.45$) ceramics are shown in Fig. 6. τ_f values linearly decreased with the increase in x. Generally, τ_f values are determined by the temperature coefficient of the dielectric constant (τ_ε) in the single-phase area, and τ_ε was calculated by using Formulas (14) and (15).[30-33]

$$\tau_f = -(\alpha + \frac{1}{2}\tau_\varepsilon) \quad (14)$$

$$\tau_\varepsilon = \frac{1}{\varepsilon_r}(\frac{\partial \varepsilon_r}{\partial T}) = \frac{(\varepsilon_r - 1)(\varepsilon_r + 2)}{3\varepsilon_r} \times \left[\frac{1}{\alpha_m}(\frac{\partial \alpha_m}{\partial V})_V + \frac{1}{\alpha_m}(\frac{\partial \alpha_m}{\partial V})_T(\frac{\partial V}{\partial T})_P - \frac{1}{V}(\frac{\partial V}{\partial T})_P\right] \quad (15)$$

where α is a constant of about 10 ppm/°C for ceramics, α_m and V represent the polarizability and

volume, respectively. Hence, τ_f values depend mainly on τ_ε. Bosman and Havinga reported[31] that the second and third terms in the square brackets of Formula (15) exhibit opposite and nearly equal magnitudes such that τ_ε values are primarily affected by the first terms, which represent the restoring forces acting on the ions. Zhou Di et al. reported that the sum of the second and third terms in the square brackets of Formula (15) is a constant (approximately 6 ppm/°C) and that τ_ε values are primarily controlled by the first terms (approximately –1 ~ –10 ppm/°C), which represent the direct dependence of polarizability on temperature.[32] Therefore, τ_ε is determined by crystal structure, such as restoring forces acting on the ions,[34] and restoring forces are positively related to octahedral distortions.[35] The τ_f values of $Ca_{1-x}Sr_xSnSiO_5$ ($0 \le x \le 0.15$) ceramics could be attributed to the SnO_6 octahedral distortion. In the single-phase area, the τ_f values exhibited the opposite variation trend comparing with the octahedral distortion, and large SnO_6 octahedral distortion corresponded to low τ_f. The τ_f values of $Ca_{1-x}Sr_xSnSiO_5$ ($0.2 \le x \le 0.45$) ceramics were affected mainly by the secondary phase. SnO_2 (τ_f = −26.7 ppm/°C) and the $SrSiO_3$ (τ_f = −65.9 ppm/°C)[20] phase with negative τ_f values could adjust the positive τ_f values (τ_f = +62.5 ppm/°C) of the $CaSnSiO_5$ phase, and a near-zero τ_f value (τ_f = −1.2 ppm/°C) was obtained at x = 0.45.

4. Conclusions

$Ca_{1-x}Sr_xSnSiO_5$ ($0 \le x \le 0.45$) and SnO_2 microwave dielectric ceramics were prepared via a solid-state reaction method. The substitution of Sr^{2+} for Ca^{2+} exerted obvious effects on the microwave dielectric properties and crystal structure of $Ca_{1-x}Sr_xSnSiO_5$ ceramics, and moderate Sr^{2+} substitution promoted grain uniformity. In a single-phase area ($0 \le x \le 0.15$), ε_r values were primarily affected by total ionic polarizability, and Sr^{2+} substitution increased the ε_r values of $Ca_{1-x}Sr_xSnSiO_5$ ceramics. $Q \times f$ values were influenced by the microstructure and relative covalency of Sn–O bonds and approached their maximum values ($Q \times f$ = 60,100 GHz) at x = 0.05. SnO_6 octahedral distortion increased with the increase in x, and large SnO_6 octahedral distortion corresponded to low τ_f. In a mulit-phase area, the relative density and ε_r values of the secondary phase determined the ε_r values of $Ca_{1-x}Sr_xSnSiO_5$ ($0.2 \le x \le 0.45$) ceramics. $Q \times f$ values changed with the content of the secondary phase, and the τ_f values of the $CaSnSiO_5$ phase were adjusted to

near zero by SnO_2 and $SrSiO_3$ with negative τ_f values. $Ca_{1-x}Sr_xSnSiO_5$ (x = 0.45) ceramic with 43.7 *w*t% $CaSnSiO_5$, 34.1 *w*t% SnO_2, and 22.2 *w*t% $SrSiO_3$ exhibited excellent microwave dielectric properties (ε_r = 9.42, $Q \times f$ = 47,500 GHz, and τ_f = −1.2 ppm/°C).

Acknowledgements

This work was supported by the National Natural Science Foundation of China (NSFC-51772107 and 61771215), Research Projects of Electronic Components and Devices of China (1807WM0004), the Major Programs of Technical Innovation in Hubei Province of China (2018AAA039), and the Innovation Team Program of Hubei Province, China (2019CFA004). The authors are grateful to the Analytical and Testing Center, Huazhong University of Science and Technology, for SEM analyses.

References

1. Xu XH, He QL, Yan L. White-light long persistent and photo-stimulated luminescence in $CaSnSiO_5:Dy^{3+}$. J. Alloy Compd. 2013;574(15):22−26.
2. Higgins JB, Ribbe PH. The structure of malayaite, $CaSnOSiO_4$, a tin analog of titanite. Am Mineral. 1977;62(7):801-806.
3. Lee G, Stefan K, Ulrich B, Claudia S, Hans GK, Hinrich M, et al. A synchrotron radiation, HRTEM, X-ray powder diffraction, and Raman spectroscopic study of malayaite, $CaSnSiO_5$. Am Mineral. 1996;81(5):595-602.
4. Zhang M, Meyer HW, Groat LA, Bismayer U, Salje EKH, Adiwidjaja G. An infrared spectroscopic and single-crystal X-ray study of malayaite, $CaSnSiO_5$. Phys Chem Miner. 1999;26(7):546-553.
5. Ghose S, Ito Y, Hatch DM. Paraelectric-antiferroelectric phase transition in titanite, $CaTiSiO_5$. Phys Chem Miner. 1991;17(7):591-603.
6. Shannon RD. Revised effective ionic radii and systematic studies of interatomic distances in halides and chalcogenides. Acta Crystallogr A. 1976;32(1):751-767.
7. Wu SP, Chen DF, Jiang C, Mei YX, Ma Q. Synthesis of monoclinic $CaSnSiO_5$, ceramics and their microwave dielectric properties. Mater Lett. 2013;91(15):239-241.
8. Du K, Song XQ, Li J, Wu JM, Lu WZ, Wang XC, et al. Optimized phase compositions and

improved microwave dielectric properties based on calcium tin silicates. J. Eur Ceram Soc. 2019;39(2-3):340-345.

9. Wu SP, Jiang C, Mei YX, Tu WP. Synthesis and microwave dielectric properties of Sm_2SiO_5 ceramics. J Am Ceram Soc. 2012;95(1):37-40.
10. Kan A, Ogawa H, Ohsato H. Synthesis and crystal structure–microwave Dielectric property relations in Sn-substituted $Ca_3(Zr_{1-x}Sn_x)Si_2O_9$ solid solutions with cuspidine structure. Jpn J Appl Phys. 2007;46(10B):7108-7111.
11. Wu SP, Chen DF, Mei YX, Ma Q. Synthesis and microwave dielectric properties of $Ca_3SnSi_2O_9$ ceramics. J Alloy Compd. 2012;521(25):8-11.
12. Colin S, Dupre B, Venturini G, Malaman B, Gleitzer C. Crystal structure and infrared spectrum of the cyclosilicate $Ca_2ZrSi_4O_{12}$. J Solid State Chem. 1993;102(1):242-249.
13. Song XQ, Du K, Zhang XZ, Li J, Lu WZ, Wang XC, et al. Crystal structure, phase composition and microwave dielectric properties of $Ca_3MSi_2O_9$ ceramics. J Alloy Compd. 2018;750:996-1002.
14. Tang Y, Xu MY, Duan L, Chen JQ, Li CC, Xiang HC, et al. Structure, microwave dielectric properties, and infrared reflectivity spectrum of olivine type Ca_2GeO_4 ceramic. J Eur Ceram Soc. 2019;39(7):2354-2359.
15. Lei W, Zou ZY, Chen ZH, Ullah B, Zeb A, Lan XK, et al. Controllable τ_f value of barium silicate microwave dielectric ceramics with different Ba/Si ratios. J Am Ceram Soc. 2017;101(1):25-30.
16. Du K, Song XQ, Li J, Lu WZ, Wang XC, Wang XH, et al. Phase compositions and microwave dielectric properties of Sn-deficient Ca_2SnO_4 ceramics. J Alloy Compd. 2019;802:488-492.
17. Rietveld HM. A profile refinement method for nuclear and magnetic structures. J Appl Cryst. 1969;2:65-71.
18. Hakki BW, Coleman PD. A dielectric resonant method of measuring inductive capacitance in the millimeter range. IRE Trans Microwave Theory Technol. 1960;8(4):402-410.
19. Song XQ, Xie MQ, Du K, Lu WZ, Lei W. Synthesis, crystal structure and microwave

dielectric properties of self-temperature stable $Ba_{1-x}Sr_xCuSi_2O_6$ ceramics for millimeter-wave communication. J Mater. 2019;5(4):606-617.

20. Ohsato H, Suzuki I, Kagomiya I. Crystal structure and microwave dielectric properties of α-$(Ca_{1-x}Sr_x)SiO_3$ (x = 1 and 0.8) ring silicates for millimeter-wave applications. J Alloy Compd. 2017;96(2):115-120.
21. Shannon RD. Dielectric polarizabilities of ions in oxides and fluorides. J Appl Phys. 1993;73(1):348-366.
22. Sebastian MT. Dielectric Materials for Wireless Communication. Elsevier. 2010.
23. Choi GK, Kim JR, Yoon SH, Hong KS. Microwave dielectric properties of scheelite (A = Ca, Sr, Ba) and wolframite (A = Mg, Zn, Mn) $AMoO_4$ compounds. J Eur Ceram Soc. 2007;27(8-9):3063-3067.
24. He H, Xu Y. A unified equation for predicting the dielectric constant of a phase composite. Appl Phys Lett. 2014;104(6):062906.
25. Brese NE, O'keeffe M. Bond-valence parameters for solids. Acta Crystallogr B. 1991;47(2):192-197.
26. Brown ID, Shannon RD. Empirical bond-strength-bond-length curves for oxides. Acta Crystallogr A. 1973;29(3):266-282.
27. Rama Rao SD, Roopas Kiran S, Murthy VRK. Correlation between structural characteristics and microwave dielectric properties of scheelite $Ca_{1-x}Cd_xMoO_4$ solid solution. J Am Ceram Soc. 2012;95(11):3532-3537.
28. Zhang Y, Zhang Y, Xiang M. Crystal structure and microwave dielectric characteristics of Zr-substituted $CoTiNb_2O_8$ ceramics. J Eur Ceram Soc. 2015;36(8):1945-1951.
29. Lei W, Ran A, Wang XC, Lu WZ. Phase evolution and near-zero shrinkage in $BaAl_2Si_2O_8$ low-permittivity microwave dielectric ceramics. Mater Res Bull. 2014;50:235-239.
30. Bosman AJ, Havinga EE. Temperature dependence of dielectric constants of cubic ionic compounds. Phys Rev. 1963;129(4):1593-1600.
31. Guo HH, Zhou D, Pang LX, Qi ZM. Microwave dielectric properties of low firing temperature stable scheelite structured (Ca, Bi)(Mo, V)O_4 solid solution ceramics for LTCC

applications. J Eur Ceram Soc. 2019;39(7):2365-2373.
32. Guo HH, Zhou D, Liu WF, Pang LX, Wang DW, Su JZ, Qi ZM. Microwave dielectric properties of temperature-stable zircon-type (Bi, Ce)VO_4 solid solution ceramics. J Am Ceram Soc. 2020;103(1):423-431.
33. Pang LX, Zhou D. Modification of $NdNbO_4$ microwave dielectric ceramic by Bi substitutions. J Am Ceram Soc. 2019;102(5):2278-2282.
34. Ramarao SD, Murthy VRK. Crystal structure refinement and microwave dielectric properties of new low dielectric loss $AZrNb_2O_8$ (A: Mn, Zn, Mg and Co) ceramics. Scripta Mater. 2013;69(3):274-277.
35. Lee HJ, Hong KS, Kim SJ, Kim IT. Dielectric properties of MNb_2O_6 compounds (where M = Ca, Mn, Co, Ni, or Zn). Mater Res Bull. 1997;32(7):847-855.

Table Captions:

Table 1 The weight percentage of secondary phase, lattice parameters, and Rietveld discrepany factors of $Ca_{1-x}Sr_xSnSiO_5$ ($0 \le x \le 0.45$) and SnO_2 ceramics sintered at their optimized temperatures.

Compositions	Phase compositions		Lattice parameter of main phase					Rietveld discrepany factors		
	Main phase	Secondary phase (*wt* %)	*a* (Å)	*b* (Å)	*c* (Å)	*β* (º)	*V* (Å^3)	R_{wp} (%)	R_p (%)	χ^2

$Ca_{1-x}Sr_xSnSiO_5$	x = 0	$CaSnSiO_5$	–	7.154	8.893	6.669	113.321	389.668	9.8	7.0	4.4
	x = 0.05	$CaSnSiO_5$	–	7.158	8.905	6.675	113.338	390.618	14.9	8.5	6.1
	x = 0.1	$CaSnSiO_5$	–	7.162	8.920	6.685	113.347	392.158	15.7	11.9	5.4
	x = 0.15	$CaSnSiO_5$	–	7.166	8.933	6.692	113.355	393.336	14.8	10.7	5.1
	x = 0.2	$CaSnSiO_5$	SnO_2 (4.8)	7.164	8.941	6.696	113.354	393.807	8.7	5.9	5.9
	x = 0.3	$CaSnSiO_5$	SnO_2 (11.4) $SrSiO_3$ (6.4)	7.167	8.954	6.703	113.366	394.912	9.0	6.1	6.2
	x = 0.4	$CaSnSiO_5$	SnO_2 (30.6) $SrSiO_3$ (15.1)	7.169	8.948	6.699	113.376	394.490	9.1	6.4	6.8
	x = 0.45	$CaSnSiO_5$	SnO_2 (34.1) $SrSiO_3$ (22.2)	7.170	8.950	6.700	113.373	394.642	8.5	6.1	5.6
SnO_2	–	SnO_2	–	4.740	4.740	3.188	–	71.623	10.9	8.1	6.1

Table 2 Bond length of $Ca_{1-x}Sr_xSnSiO_5$ ($0 \leq x \leq 0.15$) ceramics from Rietveld refinement.

d (Å)	x = 0	x = 0.05	x = 0.1	x = 0.15
Ca/Sr-O_1	2.182	2.208	2.206	2.226
Ca/Sr-O_2	2.369	2.392	2.403	2.382
Ca/Sr-O_3[1]	2.688	2.698	2.672	2.710

Ca/Sr-O_3[2]	2.457	2.470	2.467	2.473
$^{-}$R (Ca/Sr-O)	2.459	2.475	2.470	2.479
Sn-O_1	1.974	1.961	1.966	1.963
Sn-O_2	2.183	2.165	2.197	2.217
Sn-O_3	2.166	2.165	2.219	2.206
$^{-}$R (Sn-O)	2.108	2.097	2.127	2.129
Si-O_2	1.592	1.557	1.559	1.574
Si-O_3	1.611	1.609	1.605	1.576
$^{-}$R (Si-O)	1.602	1.583	1.582	1.575

$^{-}$R: the average bond length.

Table 3 T_{sint}, ρ_{rel}, and microwave dielectric properties of $Ca_{1-x}Sr_xSnSiO_5$ ($0 \leq x \leq 0.45$), SnO_2, and $SrSiO_3$ ceramics.

compositions	T_{sint} (°C)	ρ_{rel} (%)	α_D^T (Å^3)	$\varepsilon_{r\text{-}exp}$	$\varepsilon_{r\text{-}corr}$	$\varepsilon_{r\text{-}cal}$	$Q\times f$ (GHz)	τ_f (ppm/°C)	Ref.
x = 0	1450	96.7 ± 0.7	16.910	11.37 ± 0.20	11.93	8.95	44,600 ± 800	+62.5 ± 4.0	[8]
x = 0.05	1450	96.9 ± 0.4	16.964	11.51 ± 0.12	12.04	8.97	60,100 ± 700	+55.5 ± 3.2	This work

CSS

x = 0.1	1425	97.5 ± 0.2	17.018	11.61 ± 0.11	12.05	8.99	52,600 ± 600	+52.3 ± 2.1	This work
x = 0.15	1400	97.9 ± 0.4	17.072	11.69 ± 0.14	12.06	9.00	47,500 ± 800	+49.6 ± 2.2	This work
x = 0.2	1400	97.5 ± 0.3	—	11.43 ± 0.17	11.86	9.29	46,800 ± 900	+44.3 ± 3.2	This work
x = 0.3	1400	96.7 ± 0.4	—	10.94 ± 0.15	11.48	9.25	45,900 ± 600	+33.5 ± 2.7	This work
x = 0.4	1425	91.5 ± 0.6	—	9.88 ± 0.27	11.14	9.73	42,900 ± 900	+11.2 ± 3.6	This work
x = 0.45	1425	90.2 ± 0.8	—	9.42 ± 0.29	10.80	9.54	47,500 ±1100	–1.2 ± 2.4	This work
SnO_2	—	1525	65.1 ± 1.5	6.850	5.27 ± 0.33	8.03	13.09	89,300 ±1400	–26.7 ± 2.6	This work
$SrSiO_3$	—	1540	—	—	6.78	—	—	13,100	–65.9	[20]

CSS: $Ca_{1-x}Sr_xSnSiO_5$; T_{sint}: the sintered temperature.

Table 4 The SnO_6 octahedral distortion, bond valence of cation and relative covalency of cation-oxygen bonds of $Ca_{1-x}Sr_xSnSiO_5$ ($0 \leq x \leq 0.15$) ceramics.

Type	x = 0	x = 0.05	x = 0.1	x = 0.15
δ (%)	0.2021	0.2103	0.2894	0.3032
$V_{Ca/Sr}$	2.051	1.995	2.054	2.045
V_{Sn}	3.591	3.701	3.461	3.457
V_{Si}	4.252	4.480	4.490	4.578
r_c (Ca/Sr-O)	24.34%	23.96%	24.35%	24.30%
r_c (Sn-O)	53.73%	54.43%	52.88%	52.85%
r_c (Si-O)	56.15%	58.06%	58.14%	59.03%

r_c: the relative covalency.

Figure Captions:

Figure. 1 The XRD patterns of SnO_2 and $Ca_{1-x}Sr_xSnSiO_5$ ceramics sintered at their optimized temperatures.

Figure. 2 Rietveld refinement of XRD pattern for $Ca_{1-x}Sr_xSnSiO_5$ ceramics sintered at optimized temperatures: (a) x = 0.05; (b) x = 0.1; (c) x = 0.15.

Figure. 3 SEM photographs and EDS spectroscopy of thermally etched $Ca_{1-x}Sr_xSnSiO_5$ and SnO_2 ceramics sintered at optimized temperatures: (a) x = 0, 1450 °C; (b) x = 0.05, 1450 °C; (c) x = 0.1, 1425 °C; (d) x = 0.15, 1400 °C; (e) x = 0.2, 1400 °C; (f) x = 0.3, 1400 °C; (g) x = 0.45, 1425 °C; (h) SnO_2, 1525 °C.

Figure. 4 The variation tendency of $\varepsilon_{r\text{-}exp}$, α_D^T, and $\varepsilon_{r\text{-}cal}$ values of $Ca_{1-x}Sr_xSnSiO_5$ ($0 \leq x \leq 0.45$) ceramics as a function of x values.

Figure. 5 The variation tendency of $Q\times f$ values and relative covalency of Sn–O as a function of x.

Figure. 6 The τ_f values and SnO_6 octahedral distortion of $Ca_{1-x}Sr_xSnSiO_5$ ceramics sintered at optimized temperatures.

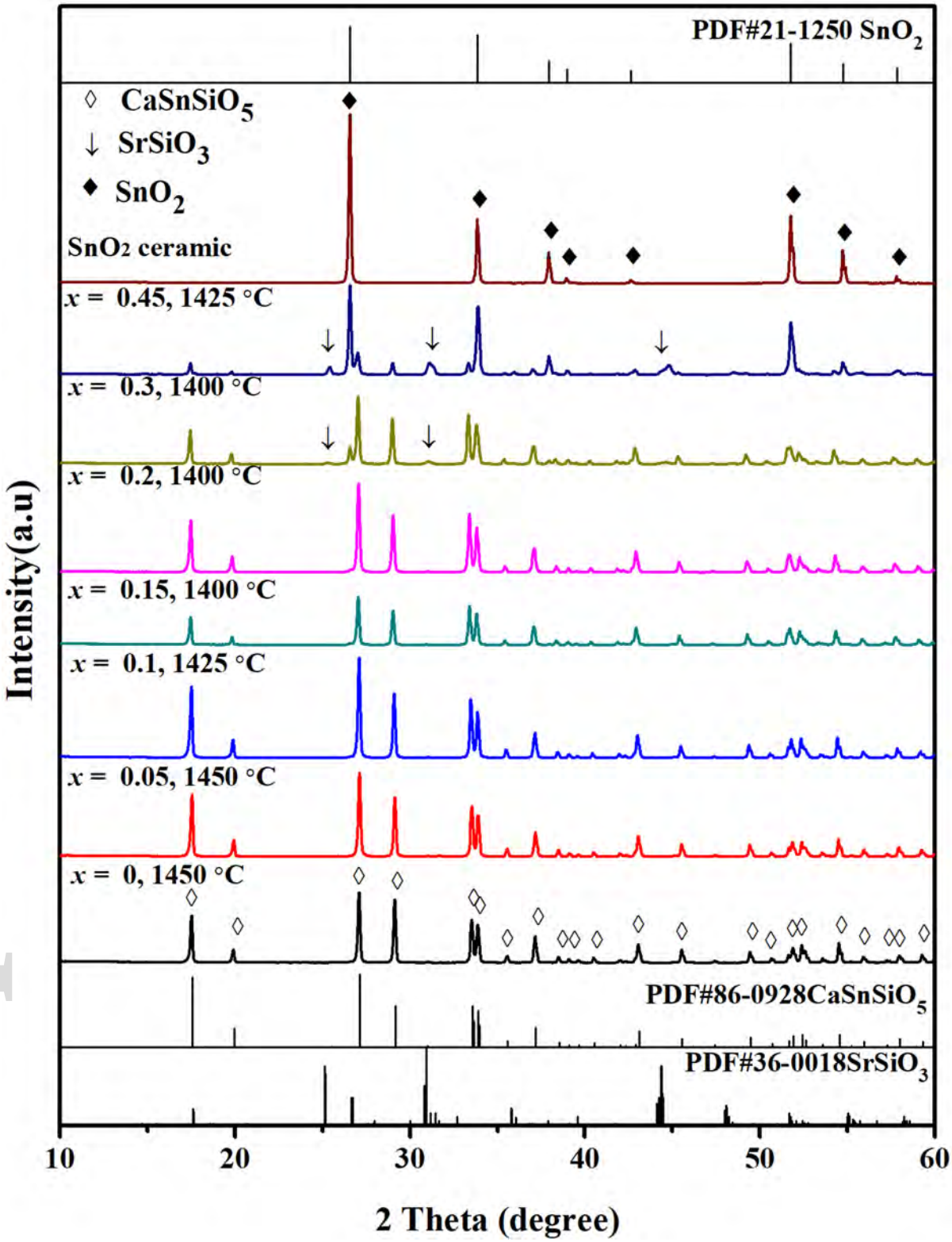

jace_17360_f1.jpg

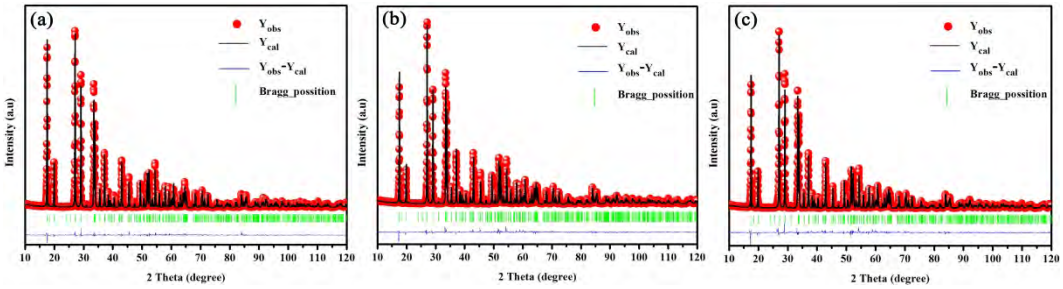

jace_17360_f2.jpg

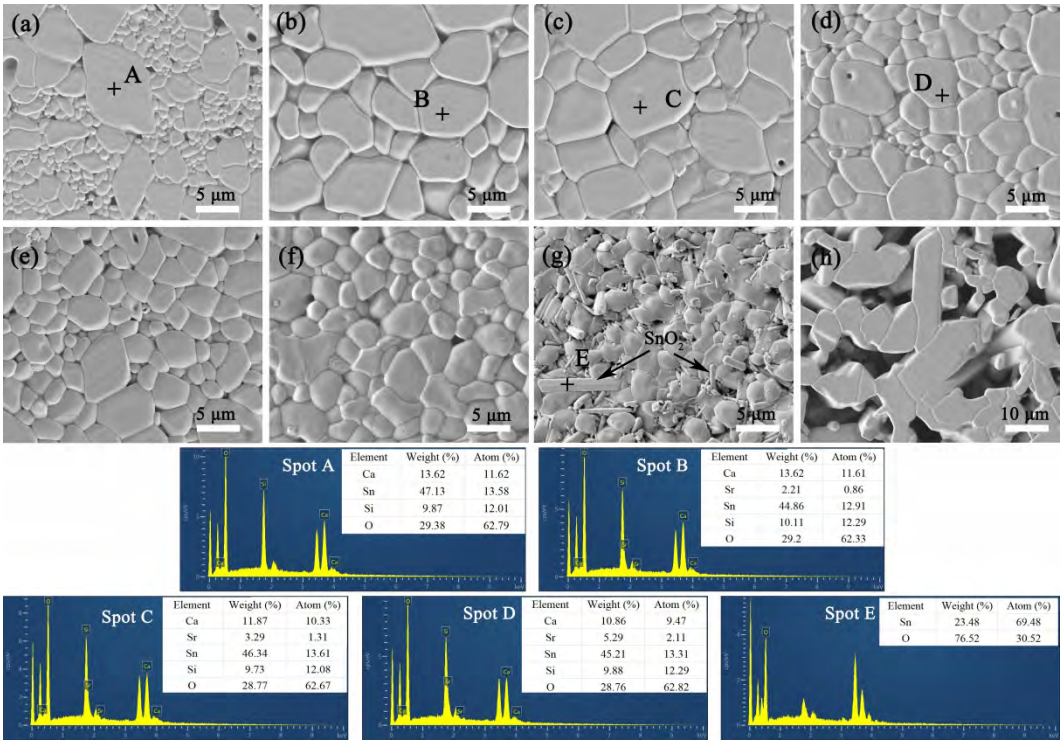

jace_17360_f3.jpg

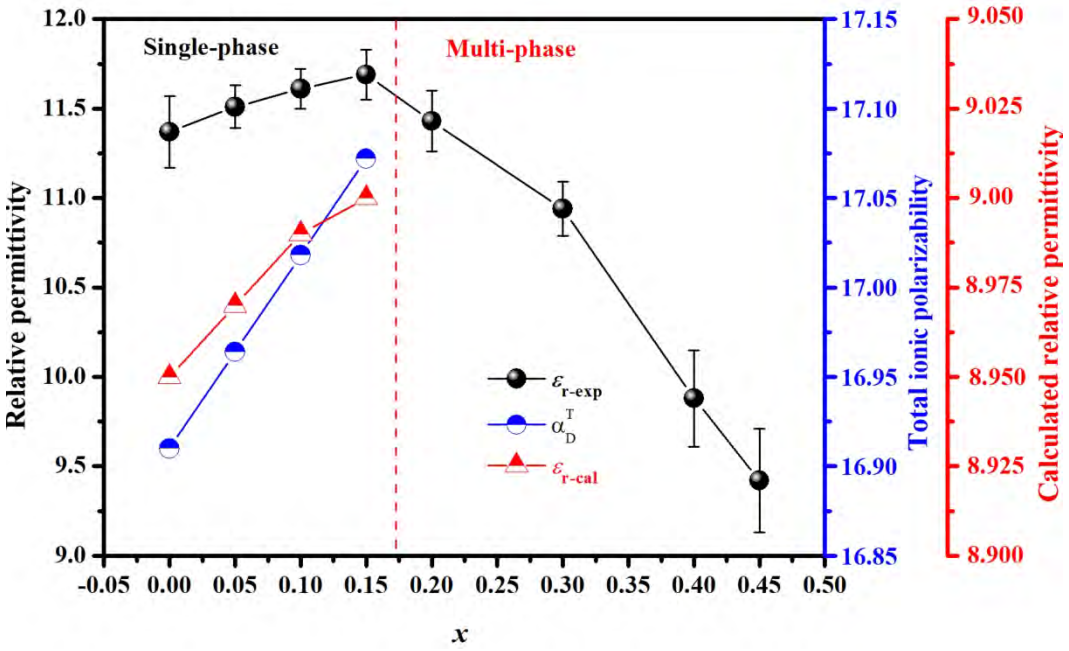

jace_17360_f4.jpg

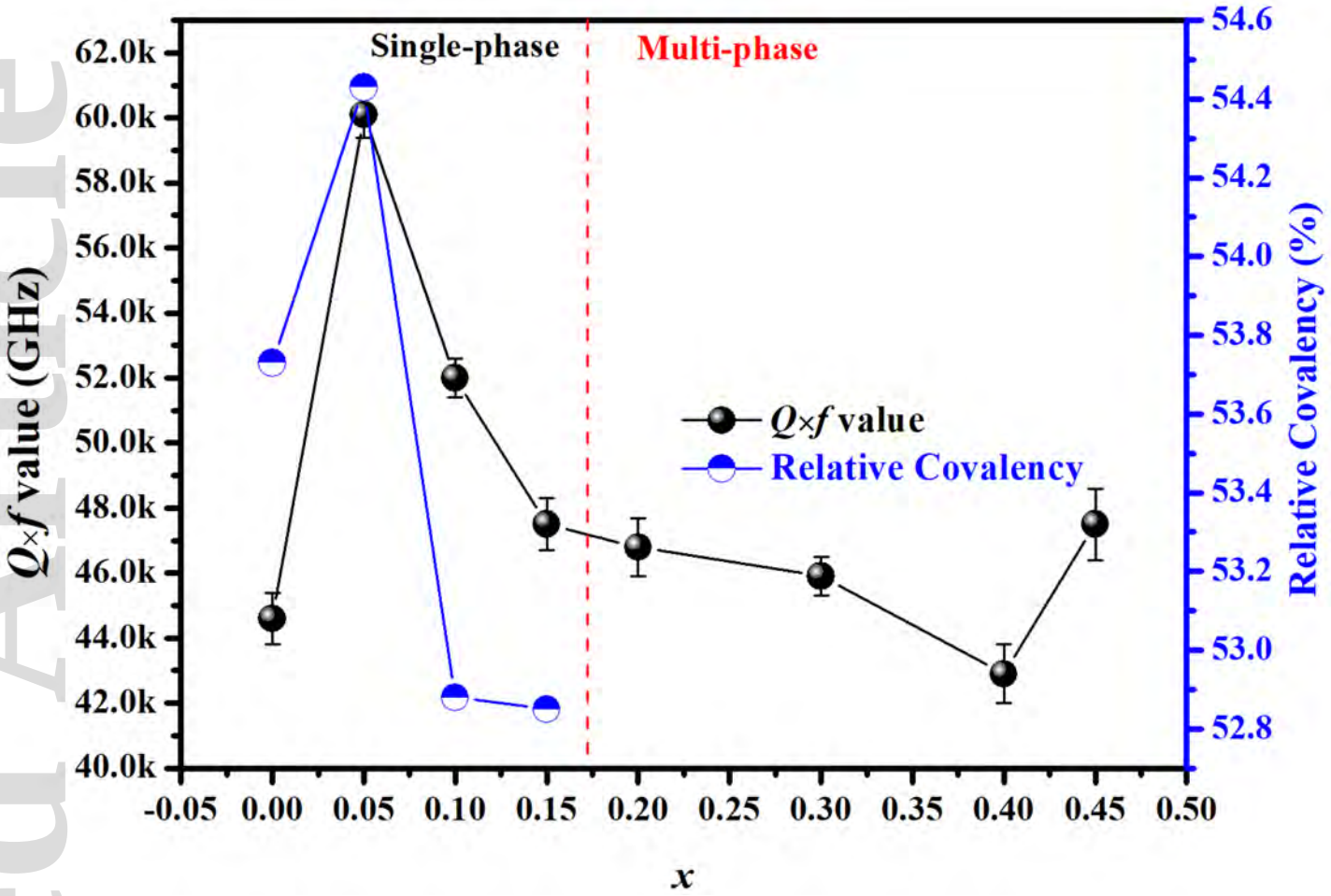

jace_17360_f5.jpg

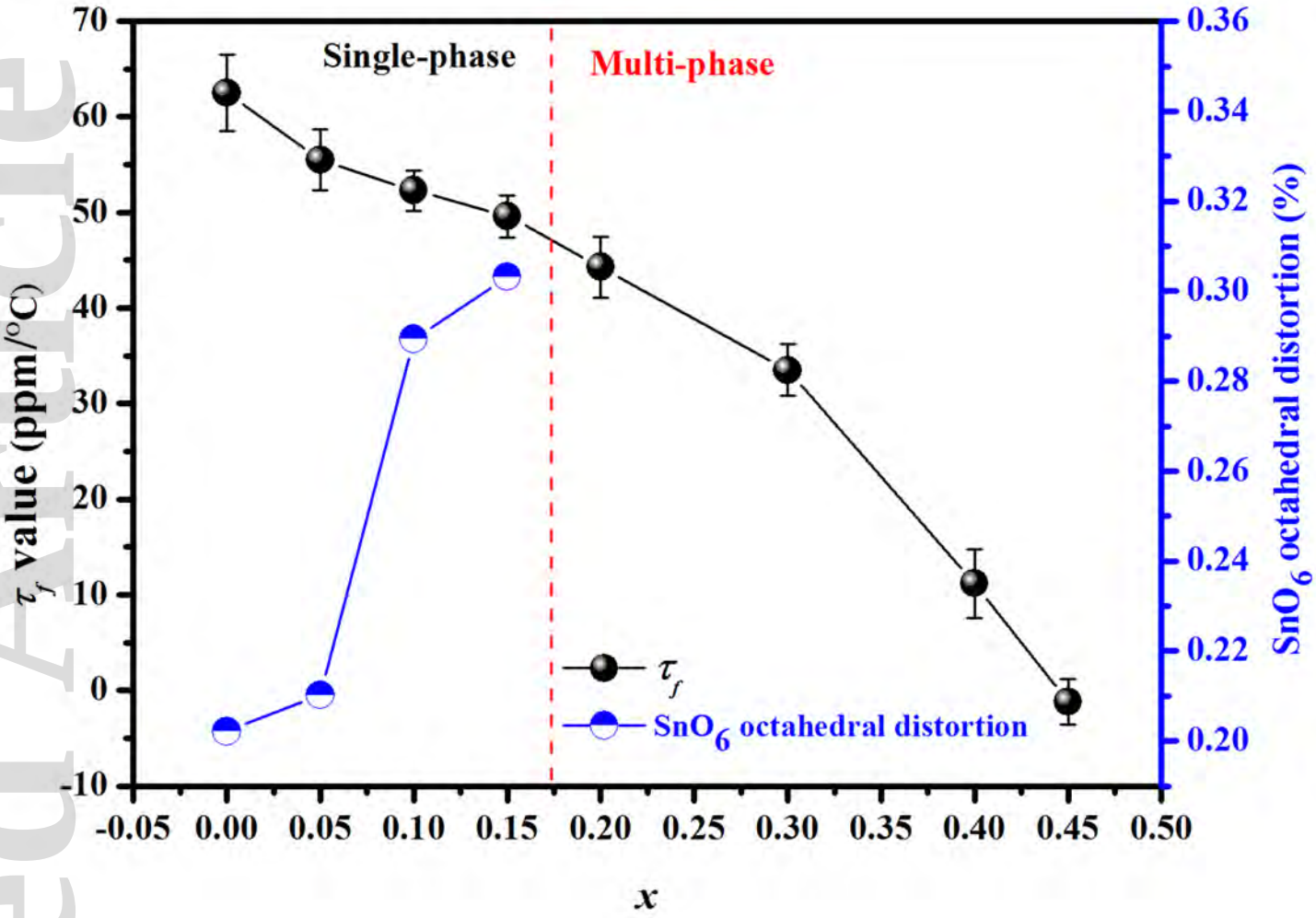

jace_17360_f6.jpg